Appl. Phys. B 72, 441–447 (2001) / Digital Object Identifier (DOI) 10.1007/s003400100501

Applied Physics B
Lasers
and Optics

Effect of patterns and inhomogeneities on the surface of waveguides used for optical waveguide lightmode spectroscopy applications

R. Horváth[1,4], J. Vörös[2], R. Graf[3], G. Fricsovszky[1], M. Textor[2], L.R. Lindvold[4], N.D. Spencer[2], E. Papp[1,*]

[1] Department of Biological Physics, Eötvös University, P.O. Box 32, 1518, Budapest, Hungary
[2] Laboratory for Surface Science and Technology, Department of Materials, ETH Zürich, Wagistrasse 2, 8952 Schlieren, Switzerland
[3] Institute for Biocompatible Materials Science and Engineering, Department of Materials, ETH Zürich, Wagistrasse 23, 8952 Schlieren, Switzerland
[4] Optics and Fluid Dynamics Department, Risø National Laboratory, P.O. Box 49, DK-4000, Roskilde, Denmark

Received: 10 July 2000/Revised version: 9 October 2000/Published online: 21 February 2001 –

Abstract. It has been found that patterns and inhomogeneities on the surface of the waveguide used for optical waveguide lightmode spectroscopy applications can produce broadening and fine structure in the incoupled light peak spectra. During cell spreading on the waveguide, a broadening of the incoupling peaks is observed, while regular microstructures on the incoupling grating produce shifts and splitting of the peaks. A theoretical model, based on the zigzag wave representation of light propagation in a planar optical waveguide has been developed in order to understand the physical background of the observed effects. Numerical results are given for the different cases observed, and they are compared with the experimental data. Several possible applications of these effects are considered.

PACS: 07.07.Df; 42.30.Lr; 42.79.Gn

Optical evanescent wave sensors are widely used for in situ monitoring of surface processes such as protein adsorption, bioaffinity interactions, formation of lipid bilayers, or cell attachment and spreading [1–3]. These sensors are based on the principle that biological adlayers on the sensor surface alter the resonant behavior of the optical system. Surface Plasmon Resonance (SPR [4]), Resonant Mirror (RM [5, 6]) and grating-coupler planar waveguides, e.g. Optical Waveguide Lightmode Spectroscopy (OWLS [7, 8]) have been developed to determine quantitatively the amount of adsorbed biomolecules on the surface. The shift in the resonance angle, determined with high precision, is often used to calculate adlayer thickness or specific coverage, generally based on the assumption of a homogeneous adlayer. In this paper, we focus on the use of the OWLS technique for studying surface inhomogeneities by demonstrating that the shape of the resonant peaks (incoupling peaks) carries information about the structures on the surface in the micron range. Using calculations based on the zigzag wave model, and treating the waveguide as a thin-film interferometer [9, 10], we analyze the changes in the shape of the resonant peaks observed during measurements with cells present. Well-defined surface structures (i.e. polymer stamps, PDMS (poly-dimethylsiloxane) for example) are used as model systems for comparison of the experimental observations with theoretical calculations.

In SPR systems, this inhomogeneity effect is well documented, and a new type of microscopy has been developed (Surface Plasmon Microscopy [11]), which is suitable for monitoring samples having extremely low contrast [12]. The inhomogeneous deformation of a plastic waveguide is the basis of Optical Force Microscopy [13, 14]. The present work explores the possibility of obtaining valuable information about the optical inhomogeneity of the sensor surface without the need for a complex microscope system. The use of well-defined, structured surfaces revealed that the observed separation of the peaks can be used for the in situ monitoring of microcontact printing (μCP) or microfluid patterning, as well as for the optical coding of complicated surface structures, such as fingerprints.

The model we have developed is based on the work of Tien and Ulrich [9, 10] and is capable of qualitatively describing the experimental results within a reasonable computational time. In the works of Morf [15] and Kunz [16], a rigorous model can be found for a similar problem.

1 Materials and methods

1.1 Materials

$Si_{0.4}Ti_{0.6}O_2$ waveguides (Microvacuum, Hungary) were used in all of the experiments. HEPES (4-(2-hydroxyethyl)piperazine-1-ethanesulfonic acid) was obtained from Fluka (Switzerland). Trypsin-EDTA and Fetal Bovine Serum (FBS) were obtained from Gibco (UK). The flow-through cuvettes used for the experiments with cells were constructed from PEEK ("Tecapeek", medical grade, Ensinger, Switzerland).The O-ring seals were from Kalrez (Flouro-Elastomer, Dupont, USA). The tubing was made of PTFE ("Teflon", Dupont, USA) and the tissue culture flask was from Nunc (Denmark).

*Corresponding author.
(Fax: +36-1/372-2757, E-mail: pappe@ludens.elte.hu)

1.2 Cell preparation

MC 3T3-E1 cells (osteogenic cell-line derived from mouse calvaria [17, 18], Department of Pathophysiology, University Bern, Switzerland) were cultured in a tissue culture flask in an alpha MEM Medium (α-MEM) containing 5% fetal bovine serum (FBS) and incubated at 37 °C under 95% air and 5% CO_2.

1.3 Optical Waveguide Lightmode Spectroscopy

The OWLS technique is based on the incoupling of He-Ne laser light into a planar waveguide via a diffraction grating. For the waveguides used in this study, the incoupling occurred at only two discrete incident angles, which represented the two polarization modes (transverse electric, TE, and transverse magnetic, TM) of the planar waveguide. The waveguide was mounted onto a rotating goniometer. The incoupled light intensity was monitored by photodiodes located at the side edges of the waveguide [19]. An example of the dependence of the incoupling intensity on the incident angle is shown in Fig. 1a for a homogeneous surface. The typical value of the peak half-width is approximately 0.04° and is determined by the optical uncertainty principle [7]. At the interface, an evanescent wave penetrated into the bulk solution up to a distance of 100–200 nm. Measuring the change in the incoupling angle allowed the direct online monitoring of the change in the effective refractive index at the surface [7]. The refractive index data could then be correlated to interface processes such as macromolecule adsorption [20, 21] or cell attachment and spreading [3]. By monitoring the changes of incoupling angle of the two waveguide modes, the refractive index changes close to the surface could be followed. Furthermore, a measuring-time resolution of 10 s allowed the online assessment of adsorption and spreading kinetics.

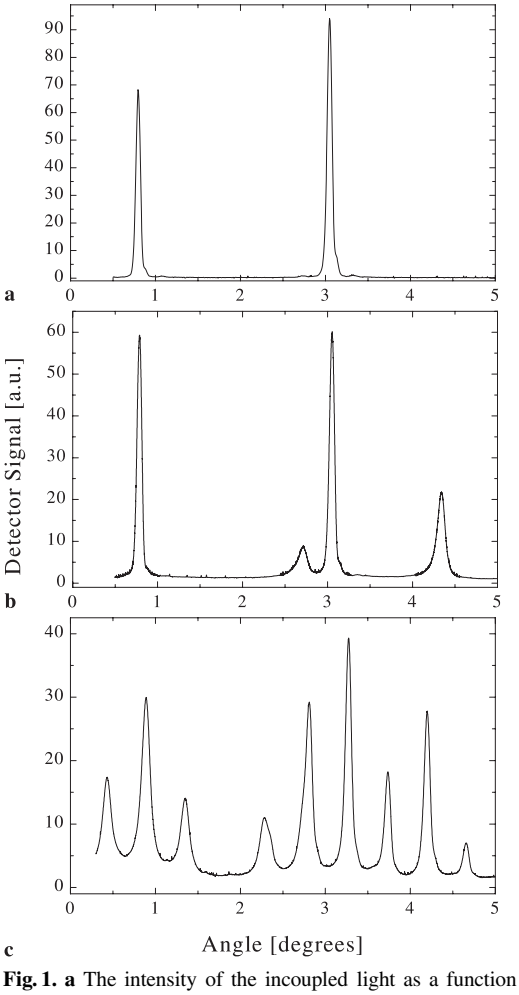

Fig. 1. a The intensity of the incoupled light as a function of the incident angle. The width of the peaks at half-maximum is about 0.04°. In this case, the incoupling angle is 0.8° for the transverse magnetic (TM) mode and 3.1° for the transverse electric (TE) mode. **b** PDMS stamp on the surface of the waveguide with grooves perpendicular to the grating. **c** PDMS stamp on the surface of the waveguide with the grooves parallel to the grating

1.4 Procedure of the cell experiments

The waveguides were exposed for 10 min to HEPES buffer (10 mM, pH 7.4). Thereafter, the waveguides were coated with serum by exposure to 100% FBS for 30 min in order to accelerate the cell attachment. The FBS solution was replaced by HEPES-buffered (25 mM) cell-culture medium containing 5% FBS (HCCM) for another 10 min. Once a steady-state OWLS signal was reached, osteoblastic cells in HCCM at a concentration of 400 000 cells/ml were introduced into the flow-through cuvette. After 10 min, a constant 1 ml/h flow of HCCM without cells was initiated and cell spreading was monitored.

After approximately 100 min, cell spreading reached a maximum. At this time, a monolayer of cells typically covered more than 70% of the waveguide surface, resulting in a steady-state signal.

1.5 Experiments with a PDMS stamp

These experiments were carried out in ambient air at room temperature. The waveguides were placed in the BIOS-1 instrument and the intensity of the incoupled light was recorded from 0.5° to 5°. Curves similar to Fig. 1a were obtained. A PDMS stamp with a groove structure of $A = 40\,\mu m$ and $B = 40\,\mu m$ (Fig. 2) was then placed on the surface of the waveguide with the grooves perpendicular to the grating and

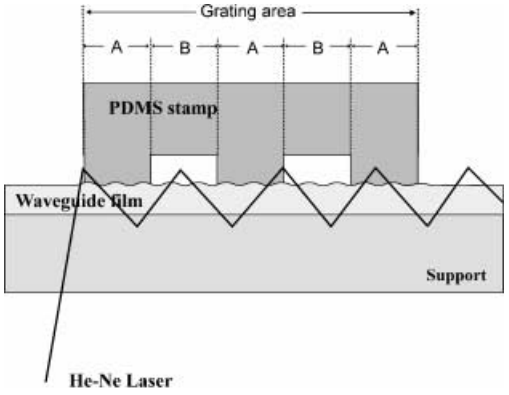

Fig. 2. The propagation of the laser light in the waveguide under the PDMS stamp

the intensity vs. angle curve was recorded again. This procedure was also repeated with the grooves parallel to the grating.

2 Experimental results

2.1 Effect of cells on the peaks

When monitoring the peak width at half-maximum (PWHM) during the process of cell spreading, we found that the PWHM increased when the cells started to spread on the surface, reached its maximum at about 50% cell coverage, and decayed back to the original level afterwards. This showed that the PWHM could be used as a measure of surface inhomogeneity. This PWHM is theoretically maximal if half of the surface is covered by cells and is minimal when either no cells are at the surface, or when the surface is completely covered by spread cells (i.e. at monolayer coverage). This increase and decrease in PWHM throughout the establishment of the cell monolayer is shown in Fig. 3.

2.2 Effect of PDMS patterns on the peaks

When a PDMS stamp with groove structures of $A = 40\,\mu\text{m}$ and $B = 40\,\mu\text{m}$ was placed at the surface of the waveguide,

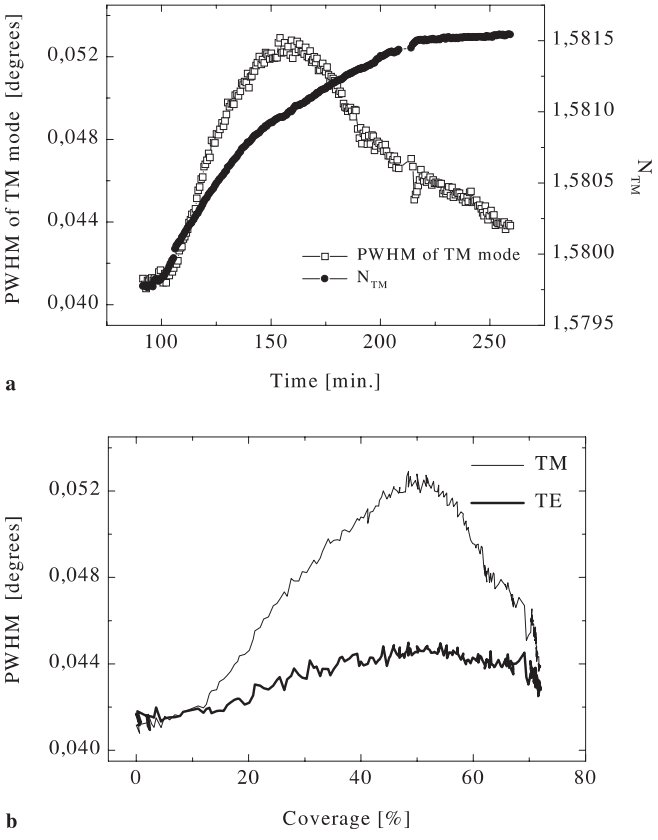

Fig. 3. a The change in the TM peak width at half-maximum (PWHM) resulting from the cell attachment. The maximum value for PWHM is observed at the time corresponding to approximately 50% surface coverage (note that the maximum effective refractive index change refers to about 75% surface coverage, see **(b)**). **b** The PWHM as a function of surface coverage due to cell attachment for both polarizations

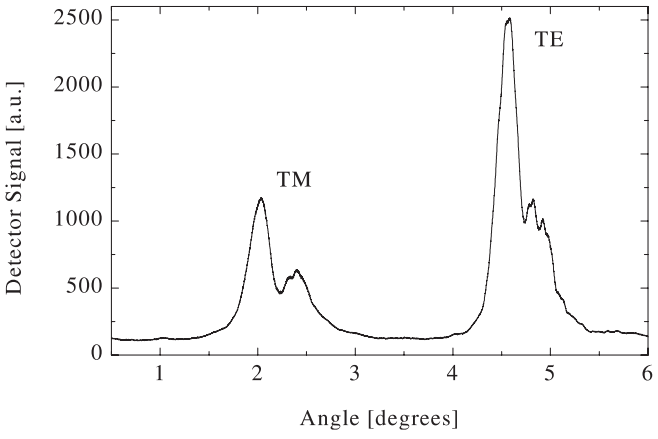

Fig. 4. Effect of fingerprints on the peaks

with the grooves perpendicular to the grating, a splitting of the peaks was observed (Fig. 1b). The refractive index was higher in the areas where the PDMS stamp touched the surface, due to the shift in incoupling in these regions to higher angles. From the difference between the original and the new incoupling angles it was possible to calculate the refractive index of the PDMS stamp. It was found to be 1.4055, as calculated from the TM peak shift. Although the ratio of PDMS-covered area to non-covered was formally one, the intensities of the peaks coupled from these areas were different. This is a consequence of the decrease in coupling efficiency when the refractive index difference between the cover media and the waveguide decreases.

When placing the same PDMS stamp on the surface of the waveguide with the grooves parallel to the grating, a more complex phenomenon was observed, with the appearance of several peaks with different intensities (Fig. 1c). Corresponding theoretical calculations are discussed in Sect. 3.

2.3 Effect of fingerprints

Experiments to monitor the effect of fingerprints on waveguides were conducted with a home-developed OWLS instrument [22]. A fingerprint was applied to the grating region of a standard waveguide chip (ASI-2400). Even if only a small part of the whole fingerprint was on the illuminated grating (size about 1 mm^2), the fine structure of both peaks could be clearly seen (Fig. 4). The result is preliminary, but this experiment demonstrates a new possibility for the optical coding of complicated surface structures.

3 Theory and numerical analysis

3.1 Coupling model for homogenous surface

Theoretical explanations for the observed effects are given in these sections, based on the zigzag wave model [9]. The guided modes propagate in the planar waveguide by total internal reflection (Fig. 5a). After having passed a full zigzag, the phase difference between the ordinary wave and the twice-reflected wave is given by:

$$\Phi \equiv 2d_F\sqrt{k^2 n_F^2 - \beta^2} + \Phi_{F,C} + \Phi_{F,S}\ . \qquad (1)$$

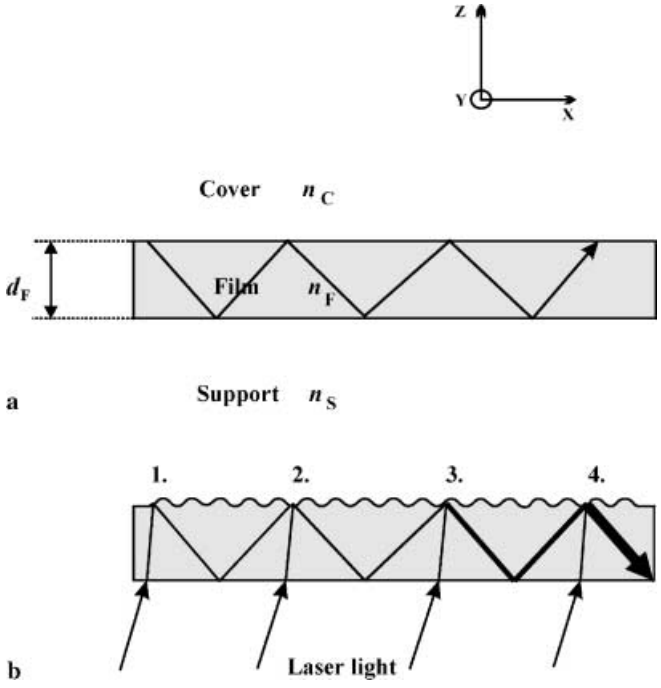

Fig. 5. a Light propagation in the planar optical waveguide by zigzag waves. **b** Coupling into the waveguide with zigzag waves

The phase shifts, after total internal reflection at the film–cover ($\Phi_{F,C}$) and at the film–substrate ($\Phi_{F,S}$) interfaces are given by (2):

$$\Phi_{F,J} = -2\arctan\left[\left(\frac{n_F}{n_J}\right)^{2p}\frac{\sqrt{\beta^2 - k^2 n_J^2}}{\sqrt{k^2 n_J^2 - \beta^2}}\right] \tag{2}$$

where $J = S, C$ (S, Substrate, or Support; C, Cover).

Here $k = 2\pi/\lambda$, where λ is the wavelength of the applied laser light in vacuum, n_F, n_S and n_C are the refractive indices of the film, substrate (support) and cover medium, respectively, and β is the x component of the wave-vector of the light in the film. The mode propagation direction in the waveguide is x (Fig. 5a) and ϱ denotes the polarization of the light: $\varrho = 0$ for TE and $\varrho = 1$ for the TM polarization modes. For a given waveguide structure and fixed polarization and wavelength, Φ is a function of β only. The mode equation of the planar waveguide thus becomes:

$$\Phi(\beta_m) = 2\pi m, \quad m = 0, 1, 2... \tag{3}$$

Here m is the mode index of the mth-guided mode. In the zigzag wave model, the mode equation is determined by self-consistency criteria: the phase shift between the ordinary wave and the twice-reflected wave must be $2\pi m$ ($m = 0, 1, 2...$). From this equation it is possible to calculate numerically β_m, the β value of the mth guided mode in the given waveguide.

In the zigzag wave model, each ray represents a plane wave [9, 10]. If the light is coupled into the waveguide, it is only necessary to consider the coupling at those points where the zigzag wave strikes the film surface, and at these points simple ray optics can be used [9].

Suppose that a plane wave enters the waveguide film (an incoming elementary ray or ordinary wave). The x wave vector component of this wave is β and its amplitude is $A_0(\beta)$. This wave excites a small wave at point 1 with amplitude $A_0(\beta)$. After a full zigzag the wave will reach point 2, where its phase has been shifted by $\Phi(\beta)$ compared to that of the ordinary wave. If the phase of this wave equals the phase of the small wave which is excited in point 2 by the ordinary wave, then the amplitudes of the two waves are additive, resulting in a wave with amplitude $2A_0(\beta)$. This wave, after a full zigzag, reaches point 3, where its phase has been shifted by $2\Phi(\beta)$ compared to the phase of the ordinary wave at this point. If its phase equals the phase of the small wave excited at point 3, a wave with an amplitude of $3A_0(\beta)$ results. This procedure can be continued through the points 4, 5, 6 etc. (Fig. 5b), resulting in a wave with 4, 5, 6 times the amplitude A_0, and with intensity 16, 25, 36 times higher than the ordinary wave intensity. Tien and Ulrich have illustrated this model for a prism coupler [10].

From the above-mentioned phase equality criterion, we arrive at the well-known condition for coupling: The x component of the wave number of the generating wave (in our case the diffracted wave from the grating) must be equal to the x component of the wave vector of one guided mode ($\beta = \beta_m$).

Provided that the phase shift during one zigzag is $\Phi(\beta)$, the amplitude of the wave after the nth zigzag, ($A_n(\beta)$), will be given by a geometrical series:

$$A_n(\beta) = A_0(\beta)\sum_{j=0}^{n-1} \mathrm{e}^{ij\Phi(\beta)} \ . \tag{4}$$

(Here and later in this paper i denotes the imaginary unit.) Using the sum equation, this can be rewritten in the form:

$$A_n(\beta) = A_0(\beta)G(\beta) \tag{5}$$

where

$$G(\beta) = \frac{\mathrm{e}^{in\Phi(\beta)} - 1}{\mathrm{e}^{i\Phi(\beta)} - 1} \ .$$

The OWLS technique uses a grating to couple the light into the waveguide. The coupling length (L) is determined by the width of the laser beam and by the width of the grating [7]. Assuming that the whole grating length is illuminated, the coupling length equals the grating length. In that case the total number, n, of the full zigzags can be calculated:

$$n = \frac{L\sqrt{k^2 n_F^2 - \beta^2}}{2d_F\beta} \ . \tag{6}$$

The intensity of the coupled light after the nth section ($I_n(\beta)$) is proportional to the absolute square of the amplitude of the light: $I_n(\beta) \sim |G(\beta)|^2$. $IG(\beta) = |G(\beta)|^2$ is introduced for this function, which gives narrow peaks at those β values representing a guided mode, i.e. at β_m ($m = 0, 1, 2...$). For a typical monomode waveguide, as used in our experiments, $IG(\beta)$ gives only one narrow peak at β_0. With increasing L, the width of this peak is decreased.

Illuminating the grating at angle α_0, the waveguide mode with β_0 is generated. The relation between β_0 and α_0 is the grating equation:

$$\beta_0 = kn_{\text{air}} \sin(\alpha_0) + \frac{2\pi}{\Lambda} \tag{7}$$

where n_{air} is the refractive index of the air and Λ is the grating periodicity [7].

Because of the finite width of the grating and the laser beam, when illuminating the grating under angle α_0 with a plane wave, the diffracted light can be described using a plane wave distribution: $A(\beta, \alpha_0)$. The $I_d(\beta, \alpha) = |A(\beta, \alpha)|^2$ function gives a peak at β_0 with a PWHM of approximately $2\pi/L$, calculated from the optical uncertainty principle [7, 21].

In the next step, the coupled light intensity has to be calculated as a function of the incident angle, $I(\alpha)$, which can also be measured using the OWLS technique. To take into account the effect of the finite length of the illuminated grating, $I(\alpha)$ will be approximated in our model with the following integral:

$$I(\alpha) \sim \int I_d(\beta, \alpha) IG(\beta) \mathrm{d}\beta \ . \tag{8}$$

For $I_d(\beta, \alpha)$, the simplest approximation of the intensity distribution of the first-order diffraction was used:

$$I_d(\beta, \alpha) = \left| \frac{\sin\left(0.5L\beta - 0.5L\left(kn_{\text{air}} \sin(\alpha) + \frac{2\pi}{\Lambda}\right)\right)}{\beta - \left(kn_{\text{air}} \sin(\alpha) + \frac{2\pi}{\Lambda}\right)} \right|^2 \ . \tag{9}$$

At a given α, (9) gives a peak at β in agreement with (7) and the PWHM of this peak is approximately $2\pi/L$. For waveguide modes, the allowable β values are between kn_S and kn_F [9]. In numerical calculations, it is sufficient to calculate the integral in (8) only in those regions where $IG(\beta)$ is relevant. It was found that the calculated shape and position of the incoupling peaks are in very good agreement with the experimental data. We found that both the calculated and the experimental curves can be approximated by a Gaussian or Lorentzian function. A Gaussian curve fit was used to determine the PWHM for all experiments and numerical calculations.

In our model, the effects of second and higher order reflected wave diffraction (i.e. the outcoupling effect) were neglected.

For modeling the inhomogeneity on the grating surface of the waveguide, the following two different situations were studied.

3.2 Coupling model with surface inhomogeneities: grooves perpendicular to the grating

In the first case, the effect of a line pattern on top of the grating is calculated for grooves oriented perpendicularly to the grating lines. If the grooves are much wider than the wavelength, the light diffraction in the y direction can be neglected. The effect of this groove structure is a phase shift at the film–cover medium interface after a total internal reflection, which is different under the covered and uncovered regions for a wave with a given β. This results in a $IG(\beta)$ function that is different for the covered and uncovered areas, denoted as $IG_c(\beta)$ and $IG_{uc}(\beta)$, respectively. $I(\alpha)$ can be approximated by the following expression:

$$I(\alpha) \sim A_c \int I_d(\beta, \alpha) IG_c(\beta) \mathrm{d}\beta + A_{uc} \int I_d(\beta, \alpha) IG_{uc}(\beta) \mathrm{d}\beta \tag{10}$$

where A_c and A_{uc} correspond to the total areas of the covered and uncovered surface. The total coupled light intensity is split into a peak corresponding to the pure chip and a second peak corresponding to the homogeneously covered chip, similar to the measured peaks given in Fig. 1b.

3.3 Coupling model with surface inhomogeneities: grooves parallel to the grating

The second case refers to a periodic line structure with the lines parallel to the grating with the assumption that the periodicity of the line pattern is much larger than the wavelength. The resulting phase shift after a total zigzag is periodically different in the waveguide film. We index the different sections with j. The phase shift after a total zigzag is Φ_j under the section j (Fig. 6).

Using the notation defined in (11) and (12):

$$G_j(\beta) = \frac{\mathrm{e}^{in_j \Phi_j(\beta)} - 1}{\mathrm{e}^{i\Phi_j(\beta)} - 1} \tag{11}$$

$$P_j(\beta) = \mathrm{e}^{in_j \Phi_j(\beta)} \tag{12}$$

where n_j is the number of total zigzags under the section j, the amplitude of the resultant wave after the *Mth* section can be calculated:

$$A_M(\beta) = A_0(\beta) \left[\sum_{j=1}^{M-1} \left[G_j(\beta) \prod_{l=j+1}^{M} P_l(\beta) \right] + G_M(\beta) \right] \tag{13}$$

where M is the number of sections in the coupling region.

In the following, the effect of alternating sections, i.e. assuming that every second section is the same, will be examined. If j is an odd number: $G_j = G_1$, $P_j = P_1$; if j is even: $G_j = G_2$, $P_j = P_2$. Suppose that $M \geq 2$ and it is even, $N = M/2$ and $P_{12} = P_1 P_2$. In this case one arrives at:

$$A_M(\beta) = A_0(\beta) G_{1,2}(\beta) \tag{14}$$

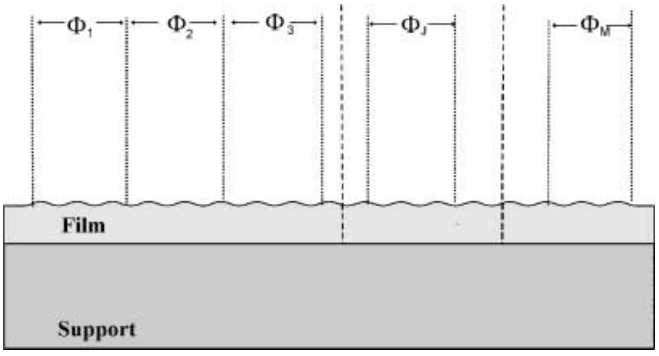

Fig. 6. The phase shifts after one total zigzag under different sections of the waveguide

where

$$G_{1,2}(\beta) = \left[(G_1(\beta)P_2(\beta) + G_2(\beta)) \left(\frac{P_{12}^N(\beta) - 1}{P_{12}(\beta) - 1} \right) \right] .$$

For a generator wave with β and amplitude $A_0(\beta)$, the intensity of the resultant wave after the *Mth* section is proportional to $|G_{1,2}(\beta)|^2$. This function is denoted by $IG_{1,2}(\beta)$. To calculate the total incoupled intensity as a function of illumination angle, α, we follow the same method as during the calculation of (8) with $IG_{1,2}(\beta)$. In this case, the total coupled light intensity is split into several peaks giving a complex peak structure (Fig. 1c).

3.4 Changes in the shape of the incoupling peaks, numerical results

To demonstrate theoretically the effect of the inhomogeneity on the grating surface of the waveguide, the results of the calculations are presented for two situations. In all calculations the following parameters have been used: $L = 0.8$ mm, $n_S = 1.525781$, $d_F = 186$ nm, $n_F = 1.7605$, $\Lambda = 416.15$ nm, $\lambda = 632.816$ nm.

3.4.1 Changes in the peak width at half-maximum (PWHM). The waveguide was homogeneously covered by a medium with $n_{c0} = 1.330$, and we began to cover the grating surface with a material of $n_c = 1.334$ (cells). The shape of the incoupling peaks was calculated for the two different polarization modes in those cases where the grating surface was covered homogeneously with n_{c0} and partly covered (10, 20, 30, 40 ... 100% of the grating area in the x direction) with n_c. Figure 7a shows the calculated incoupling peaks for TM polarization, and Fig. 7b shows the dependence of PWHM of the calculated peaks as a function of the covered area for both polarizations. In the calculations, (8) and $N = 1$ were used. The PWHM were determined by fitting a Gaussian curve to the peaks. The PWHM of the TM mode was observed to be more sensitive to surface inhomogeneities than that of the TE mode. Even with this simplified model, using homogeneous coverage for the modeling of random cell distribution, good agreement with the cell measurements was achieved (compare Figs. 7b with 3b.)

The calculated values for the PWHM of the peaks turned out to be smaller than those determined in the experiments. This can, in part, be explained by the fact that the calculations were made assuming a plane wave illumination and not taking into account the effect of the Gaussian profile of the laser beam. The unavoidable variations in the waveguide film thickness and refractive index are expected to lead to further increases in the experimental PWHM values.

3.4.2 Peak splitting due to surface structures. In order to demonstrate that a structure on the grating surface of the waveguide can cause multiple peaks, the grating surface was covered by a periodic groove structure with $n_c = 1.4055$ and $n_{c0} = 1.00026$. The periodicity of these grooves was 80 μm (Fig. 2). In Fig. 8, the calculated peak structures for the two polarization modes are shown with $N = 10$ in (8). In this case, both a shift and splitting of the peaks resulted. The result from the model calculation (Fig. 8) qualitatively describes

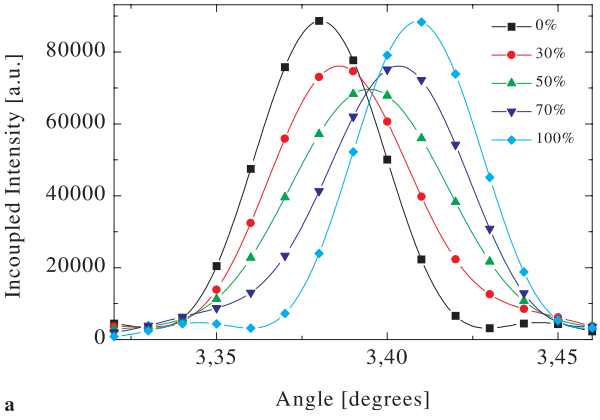

a

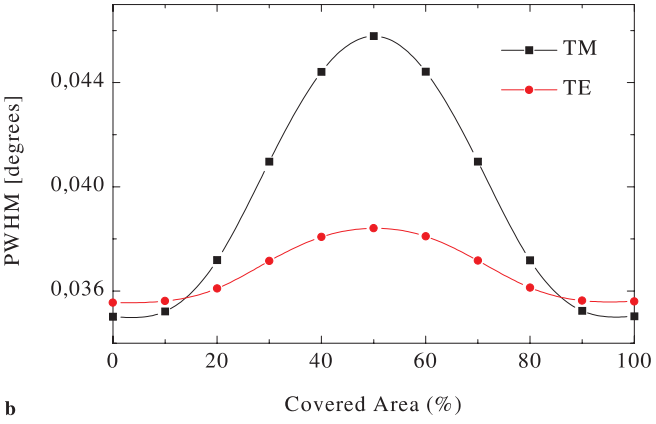

b

Fig. 7. a Calculated TM peaks from left to right: 0, 30, 50, 70, 100% coverage of the grating region. **b** Calculated width at half-maximum of the TM and TE peaks as a function of the covered area

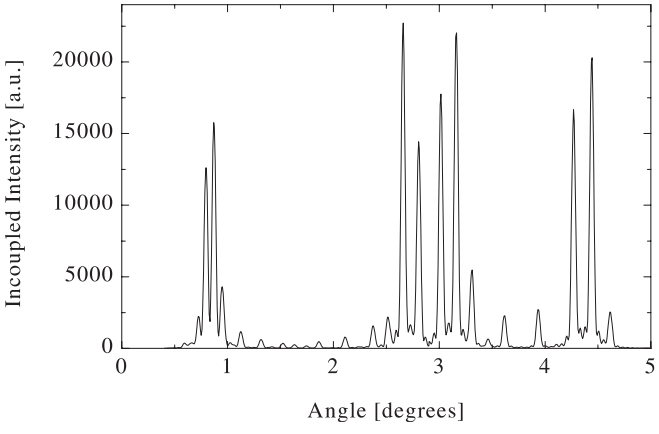

Fig. 8. The calculated peak structure (TE and TM) with the 40 micron grooves parallel to the grating lines

the experimental data (Fig. 1c). The differences can be attributed partly to some experimental uncertainties: contact of the PDMS with the film surface, and parallelism between the grooves and the grating lines. In the amplitude distribution of the peaks, differences are also expected as the model calculations do not take into account the dependence of incoupling efficiency on the cover medium refractive index (Fig. 1b), the effect of the Gaussian profile of the laser beam and the unavoidable effects of variation in the waveguide film thickness

and refractive index on the fine structure of the incoupling peaks.

4 Conclusion

This work is a first attempt to take into account the effect of inhomogeneities on waveguide performance in some specific, but applicable, situations. Surface inhomogeneities cause different effects on the incoupling peaks in OWLS experiments. Our results prove that not only the incoupling angle but also the shape and the structure of the peaks carry valuable information about the surface being analyzed. We found that inhomogeneities can generate two different effects: peak broadening and peak splitting. We have presented examples where one of these effects is the dominating factor.

Surface inhomogeneities, which do not strongly perturb the cover medium refractive index, mainly show up in the shape of the incoupling peaks. We found that the TM peak is more sensitive than the TE peak. Our model calculations give a theoretical explanation for the observed peak-broadening effect. On this basis, precise measurements (monitoring the line-shape variation and the PWHM) can give valuable information about the microstructure of the adlayer on the waveguide film.

Regular patterns on a larger scale ($\gg$ laser wavelengths) and stronger perturbation in the cover medium refractive index can result in the splitting of the incoupling peaks. These effects can be adequately described by the extended zigzag representation of light propagation in the optical waveguide. If linear patterns (e.g. grooves) are arranged in the y direction (perpendicular to the light propagation, Fig. 5a), the TM and TE peaks split (Fig. 1b), corresponding to the different cover medium refractive indices, in accordance with our model. In this case, the lines give separate channels for waveguiding, without cross talk, which can be useful in some applications such as the monitoring of microcontact printing or microfluid patterning. Linear patterns in the x direction (parallel to the light propagation in the film, Fig. 5a) result in a complex peak structure, which could be described qualitatively with our model (Figs. 1c and 8).

Large-scale irregular inhomogeneities can also produce complex peak structures, which could be a potential basis for the optical encoding of fingerprints (Fig. 4).

References

1. J.J. Ramsden: J. Stat. Phys. **73**, 853 (1993)
2. J.J. Ramsden: Phil. Mag. B **79**, 381 (1999)
3. J. Vörös, R. Graf, G. Kenausis, M. Textor, A. Bruinink, E. Wintermantel, N.D. Spencer: Biosens. Bioelectron. submitted
4. K. Welford: Opt. Quantum Electron. **23**, 1 (1991)
5. R. Cush, J.M. Cronin, W.J. Stewart, C.H. Maule, J. Molloy, N.J. Goddard: Biosens. Bioelectron. **8**, 347 (1993)
6. P.E. Buckle: Biosens. Bioelectron. **8**, 355 (1993)
7. K. Tiefenthaler, W. Lukosz: J. Opt. Soc. Am. B **6**, 209 (1989)
8. W. Lukosz: Biosens. Bioelectron. **6**, 215 (1991)
9. P.K. Tien: Rev. Mod. Phys. **49**, 361 (1977)
10. P.K. Tien, R. Ulrich: J. Opt. Soc. Am. **60**, 1325 (1970)
11. B. Rothenhausler, W. Knoll: Nature **332**, 615 (1988)
12. C.E.H. Berger, R.P.H. Kooyman, J. Greve: Rev. Sci. Instrum. **65**, 2829 (1994)
13. S. Herminghaus, M. Riedel, P. Leiderer, M. Bastmeyer, C. Strümer: Appl. Phys. Lett. **70**, 22 (1997)
14. C. Bechinger, K. Giebel, M. Schnell, P. Leiderer, H.B. Deising, M. Bastmeyer: Science **285**, 1896 (1999)
15. R.H. Morf: J. Opt. Soc. Am. A **12**, 1043 (1995)
16. R.E. Kunz, J. Dübendorfer, R.H. Morf: Biosens. Bioelectron. **11**, 653 (1996)
17. B.D. Boyan, T.W. Hummert, K. Kieswetter, D. Schraub, D.D. Dean, Z. Schwatrz: Cell. Mater. **5**, 323 (1995)
18. G.C. MacKay, R. MacNair, C. MacDonald, M.H. Grant: Biomaterials **17**, 1339 (1996)
19. R. Kurrat, M. Textor, J.J. Ramsden, P. Böni, N.D. Spencer: Rev. Sci. Instrum. **68**, 2172 (1997)
20. R. Kurrat, B. Wälivaara, A. Marti, M. Textor, P. Tengvall, J.J. Ramsden, N.D. Spencer: Colloi. Surf. B Biointerfaces **11**, 187 (1998)
21. M.F. Moreau, D. Chappard, M. Lesourd, J.P. Motheard, M.F. Basle: J. Biomed. Mater. Res. **40**, 124 (1998)
22. R. Horváth, P. Illyés, G. Fricsovszky, E. Papp: to be published